Int. J. Electrochem. Sci., 15 **(2020)** 4447 – 4453, doi: 10.20964/2020.05.04

International Journal of
ELECTROCHEMICAL
SCIENCE
www.electrochemsci.org

Short Communication

Characterization and electrical properties of a novel $Sn_{0.9}Cu_{0.1}P_2O_7/KPO_3$ composite electrolyte for intermediate temperature solid oxide fuel cells

Li Zhang, Wei Chen, Wenli Hu *

Fuyang Preschool Education College, Fuyang 236015, China
*E-mail: huwenli830914@126.com

Received: 2 January 2020 / *Accepted:* 21 February 2020 / *Published:* 10 April 2020

In this study, 10 mol% Cu^{2+}-doped SnP_2O_7 was compounded with K_2CO_3 to prepare $Sn_{0.9}Cu_{0.1}P_2O_7/KPO_3$ composite electrolyte. The structure, morphology and medium temperature electrical properties of $Sn_{0.9}Cu_{0.1}P_2O_7/KPO_3$ were investigated. The Raman spectrometer result showed that $Sn_{0.9}Cu_{0.1}P_2O_7/KPO_3$ was composed of pyrophosphate and metaphosphate groups. The maximum conductivity of $Sn_{0.9}Cu_{0.1}P_2O_7/KPO_3$ reached 6.6×10^{-2} $S\cdot cm^{-1}$ at 700 °C. The maximum power density of $Sn_{0.9}Cu_{0.1}P_2O_7/KPO_3$ reached to 131 $mW\cdot cm^{-2}$ at 700 °C.

Keywords: Pyrophosphate; Composite; Electrolyte; Conductivity; Fuel cell

1. INTRODUCTION

A fuel cell is a device which can convert the energy generated by the reaction between a fuel and oxidant into electric output in one step [1–6]. In recent years, solid oxide fuel cells (SOFCs) have attracted much attention [7–11]. Yttria doped zirconia has been widely studied and applied in solid oxide fuel cells (SOFCs). However, it must be operated at high temperatures (800–1000 °C) to obtain excellent performance. Therefore, it has become a research hotspot to explore the material systems which have superior conductivities at medium (400–700 °C) and low (100–300 °C) temperatures [12–17].

Doped pyrophosphates are considered to be appropriate materials because of their good ionic conductivities at 100–300 °C [18–20]. Singh et al. synthesized $Ce_{1-x}Sr_xP_2O_7$ and analyzed conductivity at 90-230 °C [18]. Hibino et al. found that M^{n+}-doped SnP_2O_7 had the highest conductivity among RP_2O_7 (R = Sn, Ce and Ti) materials [19–20]. Due to the low mechanical strength of single M^{n+}-doped tin pyrophosphate, composite electrolytes made of SnP_2O_7-based materials and other compounds have been developed [21–23]. Jin et al. combined $Sn_{0.95}Al_{0.05}P_2O_7$ with polybenzimidazole or polystyrene-b-poly(ethylene/propylene)-b-polystyrene to synthesize a composite membrane [21–22]. Singh et al.

synthesized new RP_2O_7 (R = Sn and Zr) / alkali carbonate composite electrolytes and found that $Sn_{0.9}In_{0.1}P_2O_7$-Li_2CO_3 had a maximum conductivity of 5.5×10^{-2} S·cm^{-1} at 630 °C [23]. Therefore, composite electrolytes can increase applied temperature ranges of SnP_2O_7-based materials. The ionic radius of Cu^{2+} (0.073 nm) is close to that of Sn^{4+} (0.069 nm). Cu^{2+} doped SnP_2O_7 composite electrolyte is an interesting research area.

In this study, a novel composite electrolyte $Sn_{0.9}Cu_{0.1}P_2O_7/KPO_3$ was prepared. The structure, morphology and medium (400–700 °C) temperature electrical properties of $Sn_{0.9}Cu_{0.1}P_2O_7/KPO_3$ were investigated.

2. EXPERIMENTAL

The calculated 2.7642 g K_2CO_3, 8.1389 g SnO_2, 13 mL 85 % H_3PO_4 and 1.8756 g $Cu(NO_3)_2$ were weighed out by analytical balance. The mixture was heated until it became gray and sticky. The primary powders were pre-fired and sintered at 500 °C and 700 °C for 1 h, respectively, to obtain the $Sn_{0.9}Cu_{0.1}P_2O_7/KPO_3$ composite electrolyte.

The crystal structure of $Sn_{0.9}Cu_{0.1}P_2O_7/KPO_3$ was determined by X-ray diffraction (XRD) and Raman spectrometer. A scanning electron microscope was used to characterize the morphology of the sintered sample. In order to analyze the conductivities, Pd-Ag paste was coated on both sides of the sintered sample and it was treated at 600 °C for 0.5 h. The AC impedance spectra of $Sn_{0.9}Cu_{0.1}P_2O_7/KPO_3$ were measured by a CHI660E electrochemical analyzer with Ag wires as the conductors. The test temperature range was 400–700 °C. Finally, hydrogen and oxygen were used as fuel and oxidant to test the fuel cell performance of $Sn_{0.9}Cu_{0.1}P_2O_7/KPO_3$.

3. RESULTS AND DISCUSSION

Fig. 1 shows the Raman spectrum of $Sn_{0.9}Cu_{0.1}P_2O_7/KPO_3$. The vibration peaks displayed near 348–404 cm^{-1} may be attributed to PO_4 tetrahedron in pyrophosphate and Cu-O-P vibration. The vibrations at 758 cm^{-1} and 1095 cm^{-1} belong to the symmetric stretching vibration of the bridged oxygen group P-O-P and the non-bridged oxygen group (PO_2) in pyrophosphate, respectively. The band at 692 cm^{-1} belongs to the symmetric stretching vibration of P-O-P in metaphosphate. The strong band at 1160 cm^{-1} belongs to the symmetric stretching vibration of the non-bridged oxygen group (PO_2) in metaphosphate [24]. The results show that $Sn_{0.9}Cu_{0.1}P_2O_7/KPO_3$ is composed of pyrophosphate and metaphosphate groups.

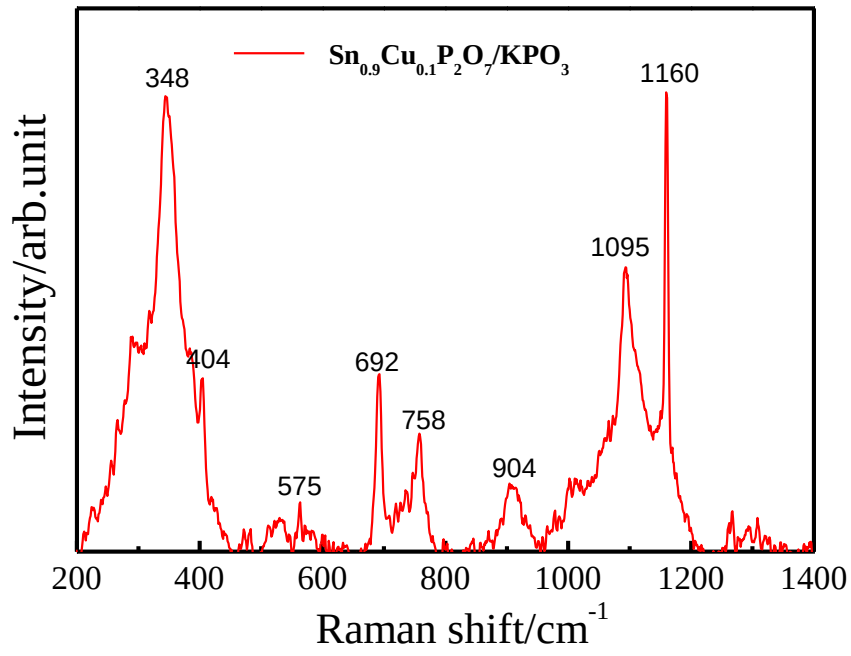

Figure 1. Raman spectrum of $Sn_{0.9}Cu_{0.1}P_2O_7/KPO_3$ composite.

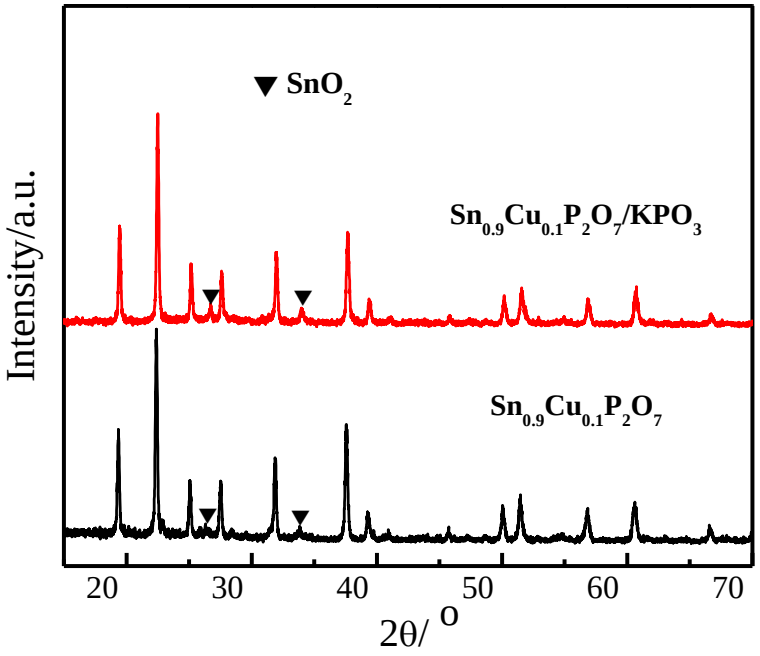

Figure 2. XRD pattern of $Sn_{0.9}Cu_{0.1}P_2O_7/KPO_3$ composite.

Fig. 2 shows the XRD diagram of $Sn_{0.9}Cu_{0.1}P_2O_7/KPO_3$. $Sn_{0.9}Cu_{0.1}P_2O_7$ is listed for comparison. The diffraction peaks of $Sn_{0.9}Cu_{0.1}P_2O_7$ are consistent with Hibino et al. [19–20]. However, there are additional weak diffraction peaks of SnO_2. It can be inferred that high heat treatment causes the loss of P element [19, 25]. For $Sn_{0.9}Cu_{0.1}P_2O_7/KPO_3$, the extra peaks appearing at 26.36° and 33.84° are obvious and they come from crystalline SnO_2. These may be due to $2H_3PO_4 + K_2CO_3 = 3H_2O + 2KPO_3 + CO_2\uparrow$

and $SnP_2O_7 + K_2CO_3 = SnO_2 + 2KPO_3 + CO_2\uparrow$ chemical reactions in the synthesis process. Combined with the Raman spectrum results, most KPO_3 exists among the grain boundaries of $Sn_{0.9}Cu_{0.1}P_2O_7$ in amorphous form.

The morphology of $Sn_{0.9}Cu_{0.1}P_2O_7/KPO_3$ is shown in Fig. 3. Fig. 3(a, b) shows that $Sn_{0.9}Cu_{0.1}P_2O_7/KPO_3$ is densified and the grains in the composite are closely combined with each other and have a clear morphology. The distribution of grains is relatively uniform. In the sintering process at 700 °C, the amorphous potassium metaphosphate can flow among the $Sn_{0.9}Cu_{0.1}P_2O_7$ particles, fill the gaps and densify the composite electrolyte.

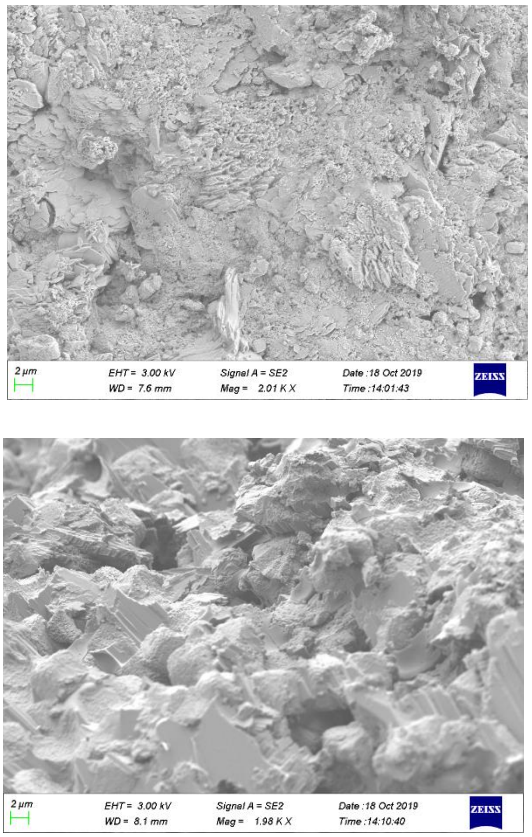

Figure 3. The external and cross-sectional SEM photos of $Sn_{0.9}Cu_{0.1}P_2O_7/KPO_3$ (a, b).

Fig. 4 shows the log (σT) ~ 1000 T^{-1} curves of $Sn_{0.9}Cu_{0.1}P_2O_7/KPO_3$ in air from 400 °C to 700 °C and the reported samples [26–27]. From Fig. 4, the conductivities of $Sn_{0.9}Mg_{0.1}P_2O_7$ (after sintered at 600 °C) at 50–250 °C are higher than those of $Sn_{0.92}In_{0.08}P_2O_7$ (after sintered at 1000 °C) at 300–700 °C [26–27]. The result shows that high sintering temperature (1000 °C) results in the deficiency of $P_2O_7^{4-}$ in $Sn_{0.92}In_{0.08}P_2O_7$ which hinders the long-range ordered conduction of ions [19]. However, there is a turning point in the Arrhenius curve of $Sn_{0.9}Mg_{0.1}P_2O_7$ at 150 °C. This shows that the electronic conductivity increases and the stability decreases in $Sn_{0.9}Mg_{0.1}P_2O_7$ above 150 °C. The conductivities of $Sn_{0.9}Cu_{0.1}P_2O_7/KPO_3$ are higher than those of single SnP_2O_7-based electrolytes in the temperature range of 400-700 °C [26–27]. This may be due to the conducting ions which could conduct through the

interface and the bulk phase in the composite. The maximum conductivity of $Sn_{0.9}Cu_{0.1}P_2O_7/KPO_3$ reached 6.6×10^{-2} S·cm^{-1} at 700 °C.

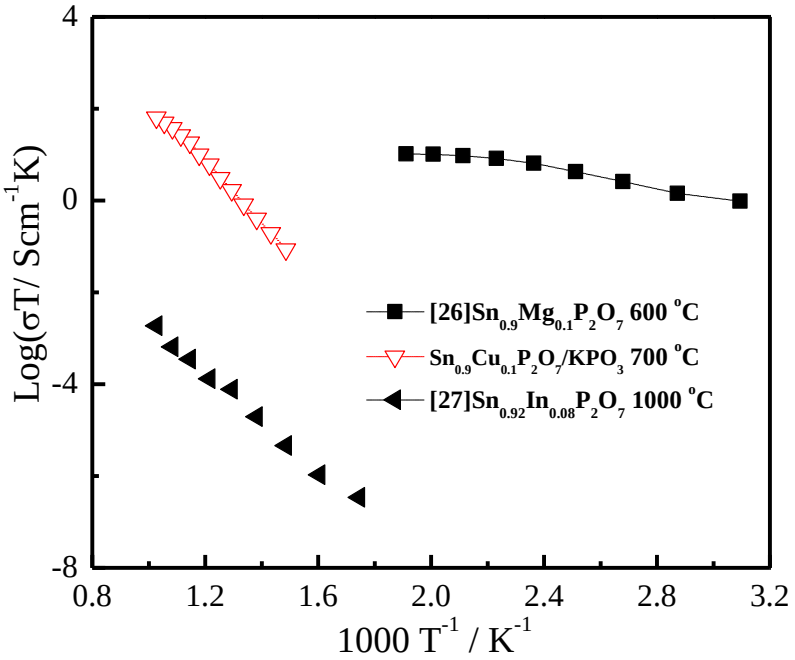

Figure 4. The log (σT) ~ 1000 T^{-1} curves of $Sn_{0.9}Mg_{0.1}P_2O_7$ (after sintered at 600 °C), $Sn_{0.9}Cu_{0.1}P_2O_7/KPO_3$ (after sintered at 700 °C) and $Sn_{0.92}In_{0.08}P_2O_7$ (after sintered at 1000 °C).

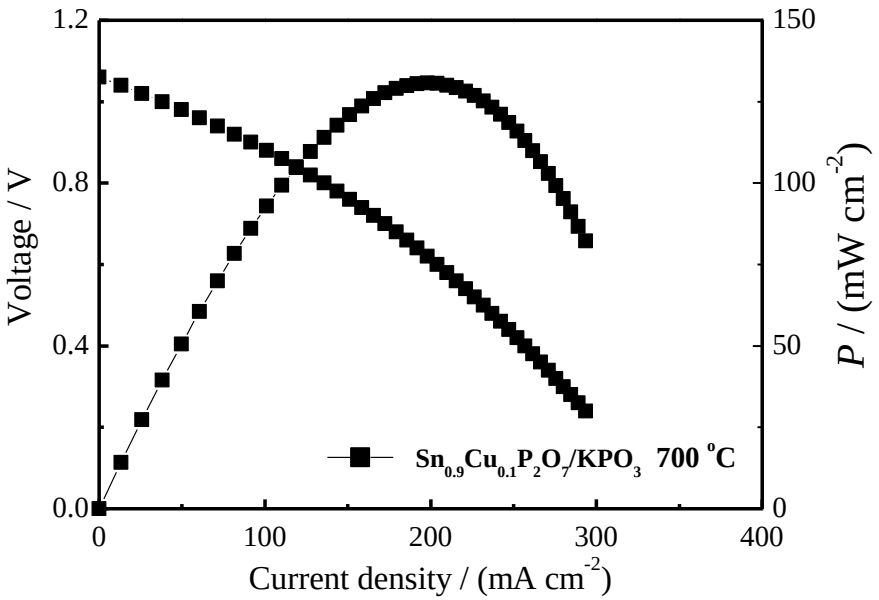

Figure 5. H_2/O_2 fuel cell performance of $Sn_{0.9}Cu_{0.1}P_2O_7/KPO_3$ at 700 °C.

Fig. 5 shows the H_2/O_2 fuel cell performance of $Sn_{0.9}Cu_{0.1}P_2O_7/KPO_3$ at 700 °C. It can be seen from Fig. 5 that the *I-V* curve is basically straight, indicating that there is no electrode polarization and the microstructure of the electrode meets the requirements. The open circuit voltage is above 1.0 V,

indicating that $Sn_{0.9}Cu_{0.1}P_2O_7/KPO_3$ is basically airtight at 700 °C. The H_2/O_2 fuel cell using $Sn_{0.9}Cu_{0.1}P_2O_7/KPO_3$ as electrolyte obtains the maximum power density of 131 $mW \cdot cm^{-2}$ at 700 °C. The value is higher than those of $Sn_{0.91}Ga_{0.09}P_2O_7$ [25], $Sn_{0.9}Mg_{0.1}P_2O_7$ [28] and $Sn_{0.94}Sc_{0.06}P_2O_7$ [29] under the same conditions (Table 1). The results show that the performance of $Sn_{0.9}Cu_{0.1}P_2O_7/KPO_3$ is good [30].

Table 1. The highest power densities of $Sn_{0.9}Cu_{0.1}P_2O_7/KPO_3$ and similar electrolytes in the literatures.

electrolytes	Highest power densities
$Sn_{0.9}Cu_{0.1}P_2O_7/KPO_3$	131 $mW \cdot cm^{-2}$, 700 °C, 1.2 mm in this work
$Sn_{0.91}Ga_{0.09}P_2O_7$	22.1 $mW \cdot cm^{-2}$, 175 °C, 1.45 mm [25]
$Sn_{0.9}Mg_{0.1}P_2O_7$	105 $mW \cdot cm^{-2}$, 150 °C, 1.0 mm [28]
$Sn_{0.94}Sc_{0.06}P_2O_7$	25 $mW \cdot cm^{-2}$, 150 °C, 1.7 mm [29]

4. CONCLUSIONS

In this study, a facile K_2CO_3 salt was compounded with 10 mol% Cu^{2+}-doped SnP_2O_7 to synthesize $Sn_{0.9}Cu_{0.1}P_2O_7/KPO_3$. The Raman spectrometer and X-ray diffraction indicated that the main structure was SnP_2O_7 phase and most KPO_3 existed among the grain boundaries of $Sn_{0.9}Cu_{0.1}P_2O_7$ in amorphous form. The SEM photos showed that $Sn_{0.9}Cu_{0.1}P_2O_7$ and KPO_3 was densified and combined with each other during the sintering process. The maximum power density of $Sn_{0.9}Cu_{0.1}P_2O_7/KPO_3$ reached 131 $mW \cdot cm^{-2}$ at 700 °C.

ACKNOWLEDGEMENTS
This work was supported by the natural science project of Anhui province of China (KJ2019A1273, KJ2018A0980).

CONFLICTS OF INTEREST
The authors declare no conflicts of interest.

References

1. L. Bi, S.P. Shafi, E.H. Da'as and E. Traversa, *Small*, 14 (2018) 1801231.
2. C. Bernuy-Lopez, L. Rioja-Monllor, T. Nakamura, S. Ricote, R. O'Hayre, K. Amezawa, M. Einarsrud and T. Grande, *Materials*, 11 (2018) 196.
3. Y.P. Xia, Z.Z. Jin, H.Q. Wang, Z.Gong, H.L. Lv, R.R. Peng, W. Liu and L. Bi, *J. Mater. Chem. A*, 7 (2019) 16136.
4. Y. Tian, Z. Lü, X. Guo and P. Wu, *Int. J. Electrochem. Sci*., 14 (2019) 1093.
5. X. Xu, L. Bi and X.S. Zhao, *J. Membrane Sci.*, 558 (2018) 17.
6. A.A. Solovyev, S.V. Rabotkin, A.V. Shipilova and I.V. Ionov, *Int. J. Electrochem. Sci*., 14 (2019) 575.

7. X. Xu, H.Q. Wang, J.M. Ma, W.Y. Liu, X.F. Wang, M. Fronzi and L. Bi, *J. Mater. Chem. A*, 7 (2019) 18792.
8. H. Jiang and F. Zhang, *Int. J. Electrochem. Sci*., 15 (2020) 959.
9. J.M. Ma, Z.T. Tao, H.N. Kou, M. Fronzi and L. Bi, *Ceram. Int.*, 46 (2020) 4000.
10. H. Dai, H. Kou, Z. Tao, K. Liu, M. Xue, Q. Zhang, L. Bi, *Ceram. Int.*, doi: 10.1016/j.ceramint.2019.11.134.
11. E. H. Da´as, L. Bi, S. Boulfrad and E. Traversa, *Sci. China Mater*., 61 (2018) 57.
12. J.-W. Ju, D.-M. Huan, Y.-X. Zhang, C.-R. Xia, G.-L. Cui, Rare Met., 37 (2018) 734.
13. Y. N. Chen, T. Tian, Z. H. Wan, F. Wu, J. T. Tan and M. Pan, *Int. J. Electrochem. Sci.*, 13 (2018) 3827.
14. T. Hibino, K. Kobayashi, P. Lv, M. Nagao, S. Teranishi, and T. Mori, *J. Electrochem. Soc.*, 164 (2017) F557.
15. H.-S. Kim, H.B. Bae, W.C. Jung and S.-Y. Chung, *Nano. Lett.*, 18(2018) 1110.
16. Z. Gong, W. Sun, Z. Jin, L. Miao and W. Liu, *ACS Appl. Energy Mater.,* 1(2018) 3521.
17. G. L. Liu, W. Liu Q. Kou and S. J. Xiao, *Int. J. Electrochem. Sci*., 13 (2018) 2641.
18. B. Singh, H-N. Im, J-Y. Park and S-J. Song, *J. Phys. Chem. C*, 117 (2013) 2653.
19. M. Nagao, T. Kamiya, P. Heo, A. Tomita, T. Hibino and M. Sano, *J. Electrochem. Soc.*, 153 (2006) A1604.
20. A. Tomita, N. Kajiyama, T. Kamiya, M. Nagao and T. Hibino, *J. Electrochem. Soc.*, 154 (2007) B1265.
21. Y.C. Jin, M. Nishida, W. Kanematsu and T. Hibino, *J. Power Sources*, 196 (2011) 6042.
22. Y.C. Jin and T. Hibino, *Electrochim. Acta*, 55 (2010) 8371.
23. B. Singh, A. Bhardwaj, S. K. Gautam, D. Kumar, O. Parkash, I.-H. Kim and S.-J. Song, *J. Power Sources*, 345 (2017) 176.
24. P. A. Bingham and R. J. Hand, *Mater. Res. Bull*., 43 (2018) 1679.
25. H. Wang, J. Liu, W. Wang and G. Ma, *J. Power Source,s* 195 (2010) 5596.
26. H. Wang, L. Sun, J. Chen and C. Luo, *Acta Phys.-Chim. Sin*., 28 (2012) 2893.
27. S. Tao, *Solid State Ionics* 180 (2009) 148.
28. K. Genzaki, P. Heo, M. Sano and T. Hibino, *J. Electrochem.Soc.,* 156 (2009) B806.
29. H. Wang, H. Zhang, G. Xiao, F. Zhang, T. Yu, J. Xiao and G. Ma, *J. Power Sources,* 196 (2011) 683.
30. Q. Guan, T. Hu, H. Wang, G. Xi, *Ceram. Int.*, doi: 10.1016/j.ceramint.2020.01.189.